



Slag corrosion characteristics of MgO-based refractories under vacuum electromagnetic field

Xinming Ren¹ · Beiyue Ma^{1,2} · Shiming Li¹ · Hongxia Li² · Guoqi Liu² · Shixian Zhao² · Wengang Yang² · Fan Qian² · Jingkun Yu¹

Received: 18 September 2018 / Revised: 22 January 2019 / Accepted: 5 February 2019 / Published online: 18 February 2019
© Australian Ceramic Society 2019

Abstract

MgO-based refractories have been widely used in metallurgical processes. However, their service lives are limited by the corrosion and penetration effects of the molten slag. To figure out the slag resistance of various MgO-based refractories, MgO–MgAl₂O₄, MgO–CaO, and MgO–C refractories were chosen in this work, and their slag corrosion characteristics under vacuum electromagnetic fields were investigated using the static crucible method at 1873 K. Furthermore, the corroded interfaces of refractories were analyzed by x-ray diffractometer (XRD), scanning electron microscope (SEM), and energy dispersive spectrometer (EDS). It was found that in CaO–Al₂O₃–SiO₂–MgO slag system, the refractories displayed different slag corrosion resistance, and their corrosion depths ranged from 3 to 10 mm. The corrosion depths of MgO–CaO refractories were more than 10 mm, which showed the worst slag resistance performance. Among them, MgO–C refractories were hardly corroded by the molten slag and its corrosion depth was less than 3 mm.

Keywords MgO-based refractories · Electromagnetic field · Corrosion · Penetration

Introduction

In consequence of the severe production environment, the attrition rate of metallurgical furnace lining is very high. Therefore, the quality of the lining material products is crucial to the entire steelmaking process. In recent years, MgO-based refractories, as a furnace lining, have been drawing much attention for its outstanding properties, such as high-melting point, excellent thermal shock resistance, and corrosion resistance [1–5].

In the past several decades, more and more studies have been developed to explain the mechanism and affecting factors of corrosion. Kiyoshi et al. [6] investigated the corrosion of MgO–MgAl₂O₄ refractories at 1723 K by calcium aluminosilicate slag. Gokce et al. [7] studied that how antioxidants

included Al, Si, SiC, and B₄C affected the oxidation resistance of MgO–C refractories and corroborated that B₄C had an exceptional performance on the oxidation resistance. In addition, some researchers also found that the slag composition has a significant effect on the corrosion resistance of refractories [8–10]. Kasimagwa et al. [11] studied the corrosion behaviors of MgO–C refractories using the rotating immersion method and found that both the stirring time and composition of liquid slag were the critical factors affecting the attrition rate of refractories. Luz et al. [12] found that a conditioned molten slag was an effective means to enhance the corrosion resistance of MgO–C materials.

Meanwhile, electromagnetism as an important auxiliary technique has been widely applied in the field of metallurgical industry, because it can improve the metal refining efficiency and products quality [13–15]. Therefore, refractories will be inevitably placed in an electromagnetic field environment. By the slag resistance experiments of MgO–C materials carried out in induction furnace and resistance furnace, Li et al. [16, 17] found the corrosion rate of MgO–C refractories was aggravated under an electromagnetic field (EMF). The effect of EMF on the formation of MgO dense layer was also investigated. However, to our knowledge, there are few reports on the slag corrosion characteristics of the MgO-based refractories under vacuum EMF.

✉ Beiyue Ma
maceramic@126.com

✉ Hongxia Li
lihongx0622@126.com

¹ School of Metallurgy, Northeastern University, Shenyang 110819, China

² State Key Laboratory of Advanced Refractories, Sinosteel Luoyang Institute of Refractories Research Co., Ltd, Luoyang 471039, China

In the present study, the slag corrosion characteristics of the MgO-based refractories, including MgO–MgAl₂O₄, MgO–CaO, and MgO–C, were investigated. Their slag resistance was evaluated adopting the static crucible method in vacuum EMF. Meanwhile, the slag corrosion characteristics were analyzed in detail.

Experimental procedures

Three types of commercially available refractory bricks were investigated in the present work, and their chemical compositions were shown in Table 1. Three experimental bricks numbered as #A, #B, and #C, respectively, which are all based on the magnesia system.

Some chemical reagents including calcium carbonate (CaCO₃), alumina (Al₂O₃), silica (SiO₂), and magnesia (MgO) were chosen to prepare the test slag (CaO–Al₂O₃–SiO₂–MgO). CaO, Al₂O₃, SiO₂, and MgO were weighed according to the mass ratio of 53:30:13:4, and then the test slag was mixed uniformly in the crucible. The basicity of the test slag is around 4.

Three kinds of MgO-based refractories were processed the crucibles with the dimension of about 60 mm × 60 mm × 90 mm (inner hole of φ30 mm × 40 mm). Then a certain amount of mixed slag was added into crucibles, and the crucibles were placed into the vacuum resistance furnace under EMF, which were heated at 1873 K for 1 h to conduct the slag corrosion and penetration tests.

In this work, static crucible method was used to study the corrosion and penetration behaviors of refractories. The refractory crucibles after corrosion test were cut along the axial direction, and then the corrosion depth and penetration depth were measured using vernier calipers. The slag resistance was evaluated by comparing the degree of corrosion and penetration.

The microstructures of crucible samples were observed via scanning electron microscopy (SEM), and different areas including corrosion layer, transition layer, and original layer were analyzed via energy dispersive spectrum analysis (EDS) to measure the contents of different elements. The macrostructures of crucible samples were observed via the photos

taken by digital camera. The apparent porosity and bulk density were measured by immersion method in kerosene under vacuum using Archimedes' principle and calculated according to Eqs. (1) and (2) [18].

$$P_a = \frac{m_3 - m_1}{m_3 - m_2} \times 100\% \quad (1)$$

$$D_b = \frac{m_1 d}{m_3 - m_2} \quad (2)$$

where P_a and D_b are the apparent porosity (%) and bulk density (g·cm⁻³) of the refractory samples; m_1 is the mass of the dried sample in air (g), m_2 is the mass of the sample in water (g), m_3 is the mass of the sample with free bubbles on the surface (g), and d is the density of kerosene (0.8 g·cm⁻³).

Results and discussion

Macrostructures

The cross-sections of crucible samples after corrosion test at 1873 K for 1 h under vacuum EMF are shown in Fig. 1. It was obvious that the corrosion depth and penetration depth of different crucible samples displayed a marked difference. That is, at the same experimental temperature and holding time, compared with sample #C (MgO–C), sample #A (MgO–MgAl₂O₄) and sample #B (MgO–CaO) displayed larger corrosion areas and deeper penetration depth on their cross-sections. Just as many cracks appeared on the cross section of sample #A due to the corrosion of slag, and the sample #B became darker because of the penetration of slag. Nevertheless, the sample #C did not show a large of changes at the cross-sections, there were some slight breaks only at the closest part of the slag. In a word, the corrosion and penetration resistance of sample #C was the best compared with sample #A and #B.

Slag corrosion depth and penetration depth

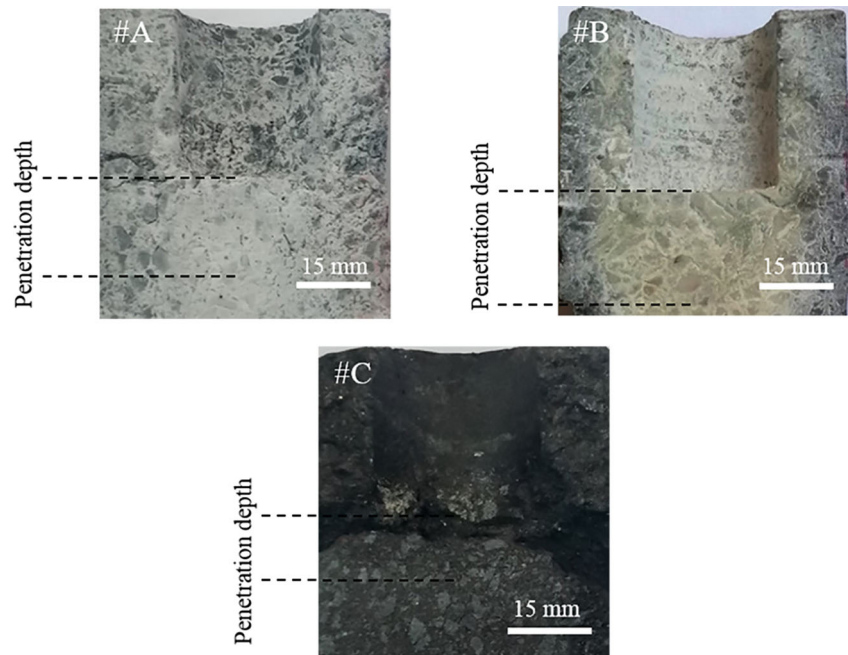
The slag corrosion depth and penetration depth of sample #A–#C after the corrosion test conducted at 1873 K for 1 h under vacuum EMF are shown in Fig. 2. As can be seen from it, among the three sets of data, the value of sample #C was the smallest both the slag corrosion depth and penetration depth. The corrosion degrees of sample #A and #B were approximate, and their penetration depth was 8 mm and 10 mm, corrosion depth was 20 mm and 24 mm, respectively. The penetration depth and corrosion depth of sample #C were the smallest, by contrast, which showed that its slag resistance was the best. Its penetration depth was only 3 mm, merely almost a third of the sample #A, and its corrosion depth was 12 mm, only half of the sample #B. It is a long-standing

Table 1 Compositions of three kinds of MgO-based refractories

Samples	Compositions (wt.%)						
	I.L.	SiO ₂	Al ₂ O ₃	Fe ₂ O ₃	CaO	MgO	C
#A (MgO–MgAl ₂ O ₄)	0.22	0.57	12.77	0.67	1.37	84.40	–
#B (MgO–CaO)	2.20	0.89	0.47	1.01	22.62	72.81	–
#C (MgO–C)	0.26	0.84	0.21	0.75	1.30	89.10	7.54

I.L. is the abbreviation for loss on ignition

Fig. 1 Crucible sections after corrosion test conducted at 1873 K for 1 h under vacuum EMF: #A—MgO–MgAl₂O₄, #B—MgO–CaO, #C—MgO–C



consensus among experts that carbon in the sample can reduce the wettability of refractories and molten slag, as well as increase the thermal conductivity at the same time [19–21]. Therefore, MgO–C refractories have an excellent slag resistance and be considered as a high-quality material applied to be as the metallurgical furnace linings.

Microstructures and elements contents

MgO–MgAl₂O₄ refractories

The SEM images and elements contents of sample #A (MgO–MgAl₂O₄ refractories) after corrosion test conducted at 1873 K for 1 h under vacuum EMF are presented in Fig. 3

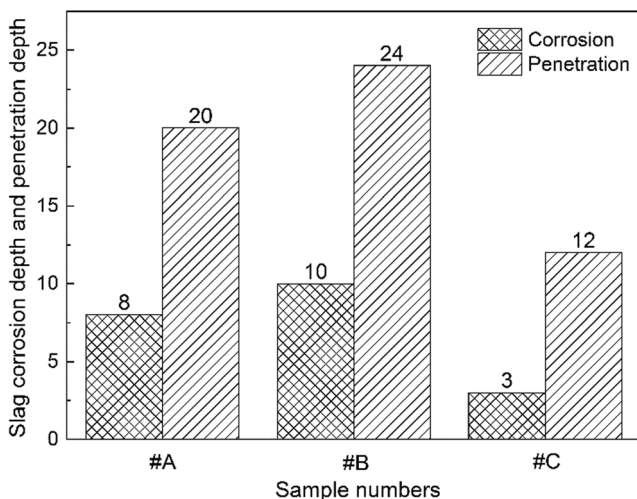


Fig. 2 Slag corrosion depth and penetration depth of different crucible samples after corrosion tested at 1873 K for 1 h under vacuum EMF: #A—MgO–MgAl₂O₄, #B—MgO–CaO, #C—MgO–C

and Table 2, respectively. It is shown in Fig. 3 that sample #A had three layers of corrosion layer (I), transition layer (II) and original layer (III). Traces of corrosion of the sample #A corrosion layer were too shallow to be observed in Fig. 3(I), it still maintains a complete interface structure. However, when the corrosion of sample #A was observed with greater magnification, some white regions including most of the slag could be seen in Fig. 3(IV), which were more evident in Fig. 3(V). It was in accord with the trend of changes in elements given in Table 2. As it is shown, from the corrosion layer to the transition layer to the original layer, the content of Al element increased and the contents of Ca and Si elements decreased. The main compositions of test slag were SiO₂ and CaO, so the white region was the slag penetrated during the corrosion test. For the corrosion layer, the contents of Al, Ca, and Si elements were the highest at point A and point C in Fig. 3(I). This is mainly because the CaO and SiO₂ in slag were left in the corrosion layer. The contents of Al, Ca, and Si elements decreased in the transition layer, which conforms to the law of corrosion. In the original layer, all elements were introduced from the unprocessed sample #A besides carbon and the contents of elements were consistent with the contents of raw materials.

MgO–CaO refractories

Table 3 shows the variation trend of elements contents of sample #B (MgO–CaO refractories) after the corrosion test, which was the same as that of sample #A. With changing from corrosion layer to transition layer to original layer, contents of Mg and O that were the main elements of sample #B increased, and contents of Al, Ca and Si elements that were

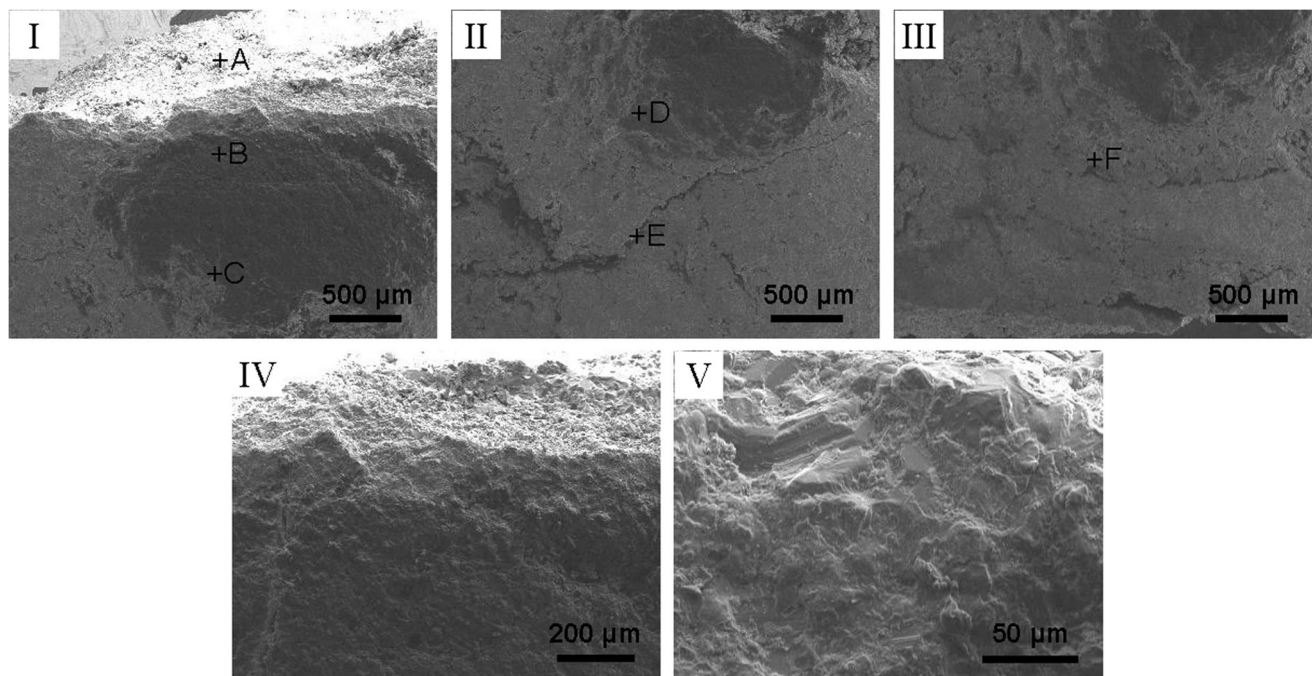


Fig. 3 SEM images of different layers of sample #A after corrosion test at 1873 K for 1 h under vacuum EMF: I—corrosion layer, II—transition layer, III—original layer, IV—corrosion layer magnified 100 times, V—corrosion layer magnified 500 times

introduced from the slag decreased. The contents of Al and Si elements achieved their maximum values at point A (8.29 wt%) and point B (3.37 wt%) in the corrosion layer, respectively. It should be noted that both the slag and sample #B contained Ca element, so the content of Ca might not accurately reflect the degrees of corrosion and penetration, and the contents of Al and Si elements were fundamental judgment criteria. The same white regions mainly composed of slag could be observed in enlargements of the corrosion layer (Fig. 4), but the original layer was not. Therefore, in the original layer, slag penetration did not occur. Besides, according to the thermodynamic data, when the temperature is over than 843 K, the existence form of Fe element will transform as follows: $Fe_2O_3 \rightarrow Fe_3O_4 \rightarrow FeO \rightarrow Fe$ [22].

Table 2 Elements contents of the sample #A analyzed by the EDS

Areas	Points	Elements contents (wt%)					
		C	O	Mg	Al	Si	Ca
Corrosion layer	A	8.32	21.64	66.53	3.51	2.38	5.82
	B	10.16	23.34	55.32	5.37	1.28	3.53
	C	11.2	21.35	56.61	7.63	–	3.21
Transition layer	D	9.52	18.35	71.69	0.44	–	–
	E	8.93	23.95	61.34	5.78	–	–
Original layer	F	4.64	27.65	54.06	8.87	0.77	4.02

The C element was introduced due to the carburization caused by the use of graphite crucible

That is the reason why the Fe element appeared in three different areas in Table 3.

MgO–C refractories

Fig. 5 and Table 4 show SEM images and elements contents of sample #C (MgO–C refractories) after the corrosion test at 1873 K for 1 h under vacuum EMF. It is found that in the corrosion layer the elemental contents obtained their maximum values, 3.08 wt% (Al), 12.50 wt% (Ca), and 4.00 wt%

Table 3 Elements contents of the sample #B analyzed by the EDS

Areas	Points	Elements contents (wt%)						
		C	O	Mg	Al	Si	Ca	Fe
Corrosion layer	A	2.99	32.73	37.55	8.29	3.37	14.56	0.51
	B	5.96	33.06	33.79	6.03	0.85	19.18	1.13
	C	6.13	31.93	35.53	4.23	–	22.18	–
	D	5.29	29.10	31.91	8.48	2.51	22.04	0.68
	E	5.05	34.98	36.91	–	2.45	20.61	–
Transition layer	F	6.68	30.97	34.15	3.39	0.99	23.63	1.18
	G	5.65	32.07	40.55	4.00	–	17.73	–
Original layer	H	6.12	33.79	36.96	2.45	–	20.14	0.54
	I	5.17	35.13	43.62	0.57	–	15.51	–
	J	7.17	34.37	42.35	0.32	0.79	15.36	0.64

The C element was introduced due to the carburization caused by the use of graphite crucible

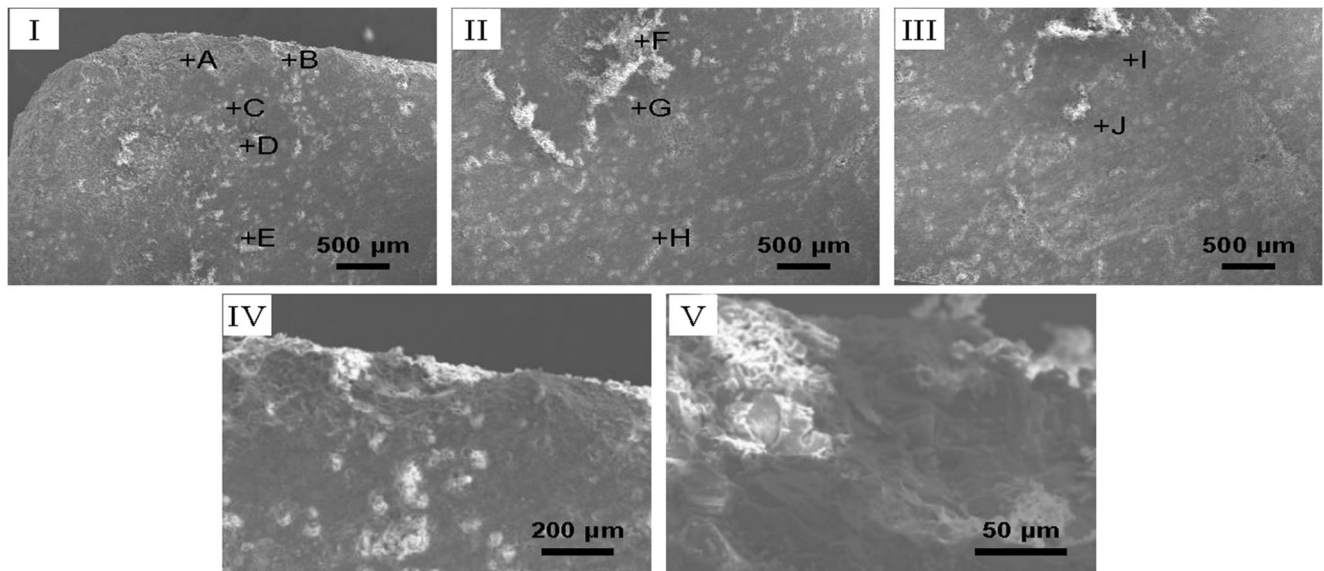


Fig. 4 SEM images of different layers of sample #B after corrosion test at 1873 K for 1 h under vacuum EMF: I—corrosion layer, II—transition layer, III—original layer, IV—corrosion layer magnified 100 times, V—corrosion layer magnified 500 times

(Si), respectively. From the corrosion layer to the transition layer to the original layer, contents of Al, Ca, and Si elements decreased whereas Mg element increased. Obviously, this change might manifest that slag penetrated into the crucible and left in the surface of sample #C by reacting with it. But it can be clearly seen that neither the transition layer nor the original layer showed an obvious change in the surface. A few impurities (white regions) were found only in the corrosion layer (Fig. 5). Impurities were from the molten slag and they could be easily proved by the analysis result of EDS in

Table 4. So the slag corrosion occurred only in the corrosion layer and a small number of slag penetration happened in the transition layer. In addition, research suggests that the carbon content in the refractories will affect their microstructures [23].

Analyses of slag corrosion and penetration behaviors

Table 5 shows the physical properties of three kinds of MgO-based refractories, including apparent porosity, bulk density,

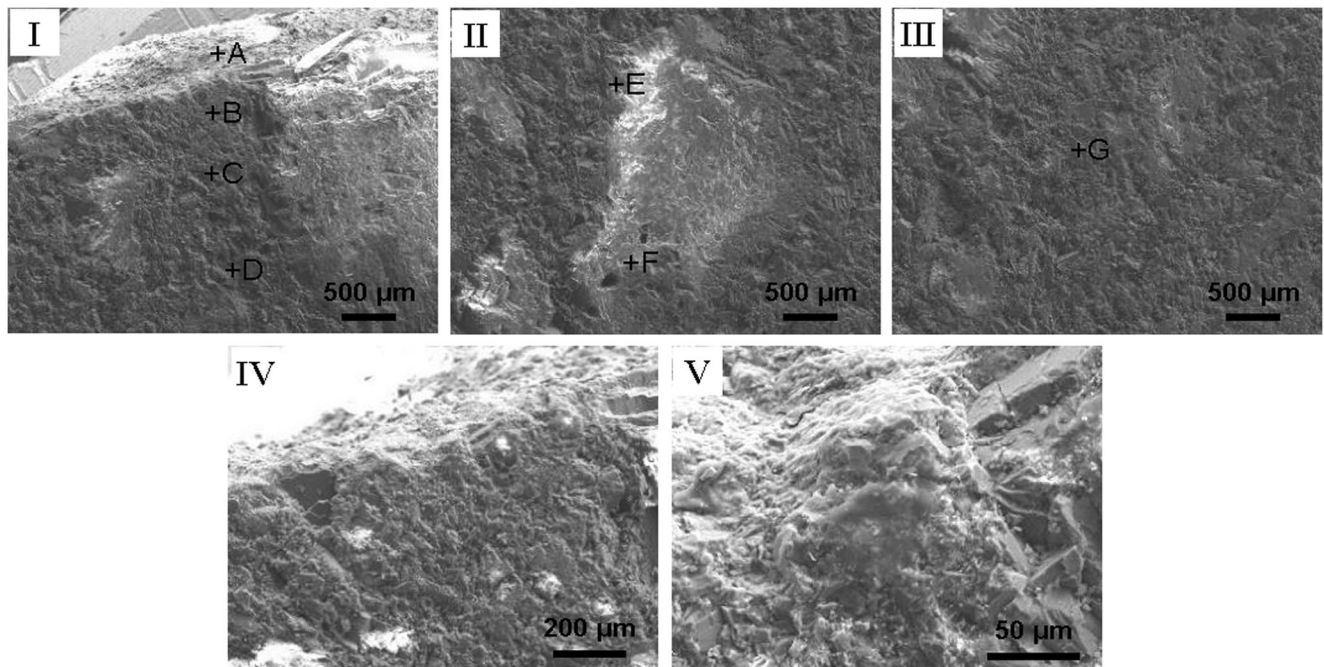


Fig. 5 SEM images of different layers of sample #C after corrosion test at 1873 K for 1 h under vacuum EMF: I—corrosion layer, II—transition layer, III—original layer, IV—corrosion layer magnified 100 times, V—corrosion layer magnified 500 times

Table 4 Elements contents of the sample #C analyzed by the EDS

Areas	Points	Elements contents (wt%)						
		C	O	Mg	Al	Si	Ca	Fe
Corrosion layer	A	14.78	30.12	27.46	3.08	1.74	10.19	1.75
	B	16.26	35.13	29.78	2.75	4.00	11.87	–
	C	21.43	30.27	31.84	0.79	1.54	12.50	1.25
	D	22.47	31.14	35.05	–	–	10.87	0.47
Transition layer	E	14.61	33.64	45.16	1.41	–	4.19	–
	F	16.25	32.8	47.02	–	0.68	2.64	0.61
Original layer	G	15.08	36.81	45.76	–	0.81	0.67	0.56

Part of the C element was introduced from the raw materials and the other due to the carburization caused by the use of graphite crucible

and cold compressive strength. It is observed that the apparent porosity of sample #A was higher than that of sample #C, and the apparent porosity of sample #B was the least, 1.5%.

Their bulk densities were reduced successively, and they were $3.41 \text{ g}\cdot\text{cm}^{-3}$, $3.15 \text{ g}\cdot\text{cm}^{-3}$, and $3.04 \text{ g}\cdot\text{cm}^{-3}$, respectively. Nevertheless, their compressive strengths increased gradually. In all the samples, the compressive strength of sample #C had the highest value, 98 MPa.

During the corrosion test, with the increase of sintering temperature, the following possible chemical reactions maybe occur:

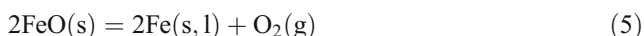
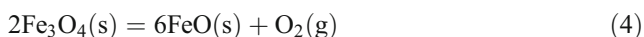
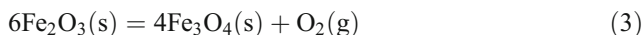


Fig. 6 shows the diagram of ΔG^0-T that might be involved in the reactions of the refractories/slag system, which includes reactions (3)–(10). It can be seen that the standard Gibbs free

energies of the reactions (3), (6)–(10) were negative when the temperature is equal to be 1873 K (it is marked with a dotted line in Fig. 6); the values of the reactions (4) and (5) were greater than zero. It shows that the reactions (3), (6)–(10) can occur spontaneously whereas the reaction (4) and reaction (5) cannot occur at this temperature. Obviously, the reaction (3) provided the oxygen source for the reactions (6) and (7). This will result in the oxidation of carbon, which will also further exacerbate the corrosion and penetration of the refractories. The content of Fe_2O_3 in three MgO-based refractories shown in Table 1 was very little, and the corrosion test was carried out under a vacuum condition, so the reaction (6) occurred at the condition of oxygen starved. It is well known that Fe_3O_4 belongs to magnetic materials, the EMF can accelerate its diffusion. This is also the reason for the poorer corrosion resistance of refractories under EMF [16, 17].

It is clear that the physical properties of the refractories were the significant difference showed in Table 5. As a consequence, this difference would be expected to result in an impact on the slag corrosion and penetration [24]. In three samples, the corrosion and penetration degrees of the sample #C were small, where the existence of about 8% carbon in the sample played an important role. Some researches indicate that the corrosion process mainly took place through the interaction between molten slag and refractories, and the penetration occurred at the open pores of refractories substrate [25, 26]. So, it is obvious that the high porosity of refractories provided more reaction zone for the slag corrosion and penetration.

Besides the physical properties such as apparent porosity and bulk density, the slag corrosion and penetration resistance of refractories also were closely associated with the components of refractories. For MgO–CaO refractories (sample #B), it performed the worst of the three kinds of refractory substrates in corrosion test. In addition to the lack of excellent physical properties, it would be easy to deduce that the main reason was the reaction of the matrix components and molten slag. In the MgO–CaO– SiO_2 and MgO–CaO– Al_2O_3 systems, a series of silicate products, like the reaction (8), were formed at the grain boundary. This leads to some low-melting compounds, such as CaAl_4O_7 , $\text{CaAl}_2\text{Si}_3\text{O}_8$, CaSiO_3 , $\text{Ca}_3\text{Si}_2\text{O}_7$, and

Table 5 Physical and mechanical properties of three kinds of MgO-based refractories

Samples	Properties		
	Apparent porosity (%)	Bulk density ($\text{g}\cdot\text{cm}^{-3}$)	Cold compressive strength (MPa)
# A (MgO– MgAl_2O_4)	17.2	3.41	55
# B (MgO–CaO)	1.5	3.15	75
# C (MgO–C)	11.1	3.04	98

MgO–CaO refractories were immersed in ceresin wax in order to prevent them to be hydrated in the storage

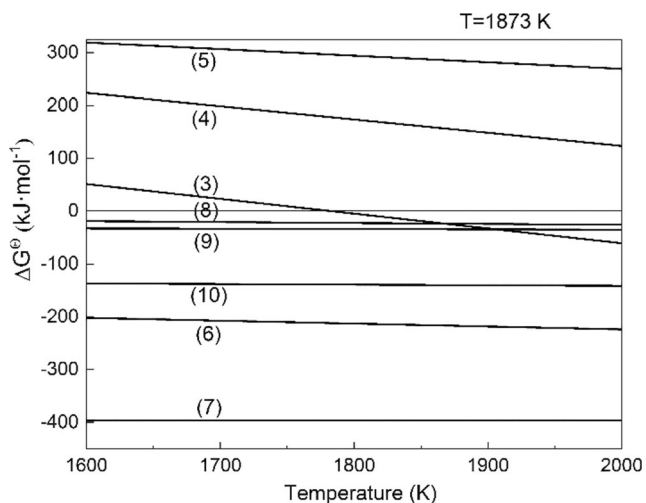


Fig. 6 Diagram of ΔG° - T for some chemical reactions in the refractories/slag system

$\text{Ca}_2\text{Al}_2\text{SiO}_7$, mingled with molten slag through open pores into the matrix and the continuity of refractories interface was destroyed, consequently, these low-melting constituents further exacerbated the corrosion and penetration [22]. However, for MgO–C refractories, the reactions of components and molten slag were beneficial to form the dense layers to prevent slag penetration. The EMF induced positive ion (Al^{3+}) of slag to migrate to the cathode and formed a high-melting spinel layer by the reaction (9). As a new protective coating, the dense spinel layer can further prevent the slag penetration [27]. In addition, the effect of the phase distribution on MgO-based refractories is not well understood currently, and this is an area warranting further study.

Conclusions

The following conclusions can be drawn from this study:

- (1) The slag resistance of MgO-based refractories depends on the properties of substrate and the composition of refractories.
- (2) EMF could aggravate the corrosion of slag to MgO-based refractories by accelerating the motion of the ions and intensifying the interface reactions.
- (3) In CaO– Al_2O_3 – SiO_2 –MgO slag system, the MgO–C refractories displayed the best slag corrosion and penetration resistance, and the depths of corrosion and penetration were 3 mm and 12 mm, respectively.

Funding information The authors gratefully acknowledge the financial supports from the open research fund for the State Key Lab for Advanced Refractories (Grant No.2016-01), National Natural Science Foundation of China (Grant No. 51772277), and the postdoctoral fund of the Sinosteel Luoyang Institute of Refractories Research Co.,Ltd.

Publisher's note Springer Nature remains neutral with regard to jurisdictional claims in published maps and institutional affiliations.

References

1. Arianpour, A.Ç., Turan, S.: Effect of calcination on the production of sintered MgAl_2O_4 by using different local waste Al_2O_3 powders. *J Aust Ceram Soc.* **53**, 975–983 (2017)
2. Sako, E.Y., Braulio, M.A.L., Zinngrebe, E., Laan, S.R.V.D., Pandolfelli, V.C.: Fundamentals and applications on *in situ* spinel formation mechanisms in Al_2O_3 –MgO refractory castables. *Ceram Int.* **38**, 2243–2251 (2012)
3. Santos, T., Luz, A.P., Pagliosa, C., Pandolfelli, V.C.: $\text{Mg}(\text{OH})_2$ nucleation and growth parameters applicable for the development of MgO-based refractory castables. *J Am Ceram Soc.* **99**, 461–469 (2016)
4. Zou, Y., Gu, H.Z., Huang, A.: Slag corrosion mechanism of lightweight Al_2O_3 –MgO castable in different atmospheric conditions. *J Am Ceram Soc.* **101**, 2029–2016 (2017)
5. Huang, A., Lian, P., Fu, L., Gu, H., Zou, Y.: Modeling and experiment of slag corrosion on the lightweight alumina refractory with static magnetic field facing green metallurgy. *J Min Metall, Sect B.* **54**, 143–151 (2018)
6. Goto, K., Argent, B.B., Lee, W.E.: Corrosion of MgO– MgAl_2O_4 spinel refractory bricks by calcium aluminosilicate slag. *J Am Ceram Soc.* **80**, 461–471 (1997)
7. Gokce, A.S., Gurcan, C., Ozgen, S., Aydin, S.: The effect of anti-oxidants on the oxidation behaviour of magnesia-carbon refractory bricks. *Ceram Int.* **34**, 323–330 (2008)
8. Dai, Y.J., Gruber, D., Harmuth, H.: Observation and quantification of the fracture process zone for two magnesia refractories with different brittleness. *J Eur Ceram Soc.* **37**, 2521–2529 (2017)
9. Korytseva, A., Navrotsky, A.: High-temperature calorimetric study of oxide component dissolution in a CaO–MgO– Al_2O_3 – SiO_2 slag at 1450 °C. *J Am Ceram Soc.* **100**, 1172–1177 (2017)
10. Muñoz, V., Camelli, S., Martinez, A.G.T.: Slag corrosion of alumina-magnesia-carbon refractory bricks: experimental data and thermodynamic simulation. *Ceram Int.* **43**, 4562–4569 (2017)
11. Kasimagwa, I., Brabie, V., Jönsson, P.G.: Slag corrosion of MgO–C refractories during secondary steel refining. *Ironmak Steelmak.* **41**, 121–131 (2014)
12. Luz, A.P., Leite, F.C., Brito, M.A.M., Pandolfelli, V.C.: Slag conditioning effects on MgO–C refractory corrosion performance. *Ceram Int.* **39**, 7507–7515 (2013)
13. Liu, Y.B., Sun, Q.J., Liu, J.P., Wang, S.J., Feng, J.C.: Effect of axial external magnetic field on cold metal transfer welds of aluminum alloy and stainless steel. *Mater Lett.* **152**, 29–31 (2015)
14. Wang, H.M., Li, G.R., Ren, Z.M., Zhao, Y.T.: Effect of exciting current of high frequency electromagnetic field on initial solidification of steel during electromagnetic continuous casting. *Ironmak Steelmak.* **36**, 615–622 (2009)
15. Zhao, Z., Chai, Y.Q., Zheng, S.H., Wang, L.S., Xiao, Y.P.: Electromagnetic field assisted metallic materials processing: a review. *Steel Res Int.* **88**, 1–11 (2017)
16. Li, X.C., Zhu, B.Q., Wang, T.X.: Effect of electromagnetic field on slag corrosion resistance of low carbon MgO–C refractories. *Ceram Int.* **38**, 2105–2109 (2012)
17. Li, X.C., Zhu, B.Q., Wang, T.X.: Electromagnetic field effects on the formation of MgO dense layer in low carbon MgO–C refractories. *Ceram Int.* **38**, 2883–2887 (2012)
18. Ren, X.M., Ma, B.Y., Zhang, Y.R., Zhu, Q., Li, D.X., Li, S.M., Yuan, L., Yu, J.K., Liu, G.Q., Li, H.X.: Effects of sintering temperature and V_2O_5 additive on the properties of SiC– Al_2O_3 ceramic foams. *J Alloys Compd.* **732**, 716–724 (2018)

19. Torre, Á.G.D.I., Valle, F.J., Aza, A.H.D.: Direct mineralogical composition of a MgO–C refractory material obtained by Rietveld methodology. *J Eur Ceram Soc.* **26**, 2587–2592 (2006)
20. Bag, M., Adak, S., Sarkar, R.: Study on low carbon containing MgO–C refractory: use of nano carbon. *Ceram Int.* **38**, 2339–2346 (2012)
21. Bag, M., Adak, S., Sarkar, R.: Nano carbon containing MgO–C refractory: effect of graphite content. *Ceram Int.* **38**, 4909–4914 (2012)
22. Chen, Z.Y.: *Chemical thermodynamics of refractories*. Metallurgical industry press, Peking (2005)
23. Zhu, T.B., Li, Y.W., Sang, S.B., Jin, S.L., Wang, H.: Formation of hollow MgO-rich spinel whiskers in low carbon MgO–C refractories with Al additives. *J Eur Ceram Soc.* **34**, 4425–4432 (2014)
24. Bahtli, T., Aksel, C., Kavas, T.: Corrosion behavior of MgO–MgAl₂O₄–FeAl₂O₄ composite refractory materials. *J Aust Ceram Soc.* **53**, 1–8 (2017)
25. Vázquez, B.A., Pena, P., Aza, A.H.D., Sainz, M.A., Caballero, A.: Corrosion mechanism of polycrystalline corundum and calcium hexaluminate by calcium silicate slags. *J Eur Ceram Soc.* **29**, 1347–1360 (2009)
26. Ma, B.Y., Yin, Y., Zhu, Q., Zhai, Y.Y., Li, Y., Li, G.Q., Yu, J.K.: Slag corrosion and penetration behaviors of MgAl₂O₄ and Al₂O₃ based refractories. *Refract Ind Ceram.* **56**, 494–501 (2016)
27. Díaz, L.A., Torrecillas, R., Aza, A.H.D., Pena, P.: Effect of spinel content on slag attack resistance of high alumina refractory castables. *J Eur Ceram Soc.* **27**, 4623–4631 (2007)